ASSESSMENT OF RANS TURBULENCE MODELLING APPROACHES FOR POLLUTANT DISPERSION IN VEGETATED STREET CANYONS USING PERIODIC BOUNDARY CONDITIONS

Bálint PAPP [1], Ildikó TROLL [2], Gergely KRISTÓF [3]

[1] Corresponding Author. Department of Fluid Mechanics, Faculty of Mechanical Engineering, Budapest University of Technology and Economics. Address: Műegyetem rkp. 3., H-1111 Budapest, Hungary. E-mail: papp.balint@gpk.bme.hu.
[2] Department of Fluid Mechanics, Faculty of Mechanical Engineering, Budapest University of Technology and Economics. Address: Műegyetem rkp. 3., H-1111 Budapest, Hungary. E-mail: ildikotroll@edu.bme.hu.
[3] Department of Fluid Mechanics, Faculty of Mechanical Engineering, Budapest University of Technology and Economics. Address: Műegyetem rkp. 3., H-1111 Budapest, Hungary. E-mail: kristof.gergely@gpk.bme.hu.

ABSTRACT

Although trees provide shade for pedestrians, enhancing their thermal comfort, dense vegetation can remarkably hinder the ventilation efficiency of an urban area, resulting in greater pedestrian exposure to traffic-related air pollutants. In the present paper, the widely used realizable k-ε and k-ω SST turbulence models, as well as a novel geometry-informed k-ε turbulence model are compared and applied to investigate the impact of tree planting in finite-length street canyons of $H/W = 0.5$ and $L/H = 5$ aspect ratios.

The geometry-informed k-ε model is based on a new eddy viscosity formulation that relies on the same set of physical parameters as the k-ω SST model. The new model constrains the growth of the turbulent length scale by incorporating wall distance, even in flow regions where turbulent kinetic energy dissipation exceeds production (dissipative regime). The geometry-informed (GI) model is implemented in ANSYS Fluent as a user-defined eddy viscosity formulation for the standard k-ε model. The resulting GI k-ε model is parameterized similarly to the standard k-ε model, except for the $C_{1\varepsilon}$ constant, which is set to 1.55. The model has previously demonstrated superior accuracy compared to classic eddy viscosity models in some test cases (i.e., channel flow, shear flow, and backward-facing step), though it has not yet been tested in any complex flows.

The present paper proves that the new turbulence model is suitable for the accurate simulation of building-scale transport processes: the validation metrics, characterizing the agreement of the modelled velocity and concentration field with previous measurement data, show similar performance compared to those obtained using the industry standard realizable k-ε and k-ω SST turbulence models.

Keywords: CFD, pollutant dispersion, street canyon, trees, turbulence model, urban air quality.

NOMENCLATURE

Roman symbols

c	kg/m³	concentration
c^*	1	normalized concentration
$C_{1\varepsilon}$	1	model constant of the k-ε model
c_d	1	drag coefficient
$C_{\varepsilon4}$	1	model constant of the vegetation model
$C_{\varepsilon5}$	1	model constant of the vegetation model
D_t	m²/s	turbulent mass diffusivity
H	m	building height (reference height)
k	m²/s²	turbulent kinetic energy (TKE)
K_s	m	equivalent sand-grain roughness (wall roughness)
L	m	canyon length
L_s	m	source length
N	1	number of elements
O	[SI]	reference data observed in the experiments
P	[SI]	model predictions (CFD results)
Q	kg/m³	total source intensity
Re	1	Reynolds number
Sc_t	1	turbulent Schmidt number
S_k	kg/m/s³	vegetation source term in the equation for TKE
$S_{u,i}$	N/m³	vegetation source terms in the momentum equation
S_V	kg/m³/s	volume source intensity of the passive scalar
S_ε	kg/m/s⁴	vegetation source term in the equation for turbulent dissipation
u	m/s	streamwise velocity component

U_∞	m/s	free-stream velocity (reference velocity)
v	m/s	spanwise velocity component
$\mathbf{v}$	m/s	velocity vector
V_s	m³	volume of the source zone
W	m	canyon width (street width)
w	m/s	vertical velocity component
x	m	streamwise coordinate
y	m	spanwise coordinate
y^+	1	dimensionless wall distance
z	m	vertical coordinate

Greek symbols

β_d	1	model constant of the vegetation model
$\beta_p,$	1	model constant of the vegetation model
δ	m	boundary layer depth
Δc^*	%	change of the normalized concentration
Δx	m	mesh resolution
ε	m²/s³	dissipation rate of the TKE
v	m²/s	kinematic viscosity
v_t	m²/s	turbulent viscosity
ρ	kg/m³	air density
ω	m²/s³	specific dissipation rate of TKE

Further notations

$\overline{(X)}$	average of a data set X
σ_X	standard deviation of the data set X
$\lvert\mathbf{x}\rvert$	absolute value of the vector $\mathbf{x}$

1. INTRODUCTION

Air pollution is a significant environmental factor influencing human health, as it presents considerable hazards for pollution-related diseases and premature death. In light of urbanization, it is crucial to gain a comprehensive understanding of the flow dynamics within urban landscapes, as well as the dispersion patterns of pollutants. Moreover, it is essential to analyze the effects of vegetation and various obstructions on pollutant concentration levels, as such insights are vital for the development of reliable methods for urban air quality evaluation.

Urban vegetation, particularly trees, plays a crucial role in the microclimate of municipal areas. Trees mitigate urban heat by providing shade, leading to improved heat comfort and reduced ambient and surface temperatures (Salmond et al., 2016). By reducing runoff, trees help moderate the vulnerability to water flooding. Through intercepting precipitation and facilitating evapotranspiration, vegetation enables better adaptation to the challenges of climate change (Gill et al., 2008). Additionally, tree canopies act as pollutant sinks through dry deposition and absorption (Janhäll, 2015), and can also attenuate traffic noise. Moreover, enhancing urban vegetation supports biodiversity (Gómez-Baggethun et al., 2013) and promotes well-being by

encouraging physical activity, stress relief, cognitive restoration, and social interaction (Salmond et al., 2016).

However, trees in street canyons can adversely impact air quality by reducing airflow and trapping pollutants. Over the past two decades, several wind tunnel experiments and computational fluid dynamics (CFD) simulations have examined the aerodynamic effects of urban vegetation, which is reviewed by Janhäll (2015), Gallagher et al. (2015) and Buccolieri et al. (2018). The key findings from the relevant studies are summarized below.

Several researchers have investigated the impact of urban trees at the scale of a single street canyon. Fellini et al. (2022) and Carlo et al. (2024) used wind tunnel measurements, while Buccolieri et al. (2009) combined wind tunnel experiments with numerical simulations to analyze the effects of trees in a street canyon with a height-to-width ratio of 0.5, focusing on perpendicular wind directions. The results obtained by Buccolieri et al. (2009) indicate that trees reduced flow rates by 33% at pedestrian height compared to the empty reference canyon and despite the increased shear within the canyon, caused by the three canopy zones, TKE production remained mostly unchanged. In terms of pollutant concentrations, Fellini et al. (2022) reported an increase of up to 22% for the entire canyon volume. Meanwhile, Buccolieri et al. (2009) found that wall-averaged concentrations increased by 40% on the leeward side but decreased by 25% on the windward side in the presence of trees. Noteworthy results from Fellini et al. (2022) showed that the average pollution level does not correlate with the number of trees, contradicting the belief that an increased vegetation fraction leads to an increased pollutant accumulation. The evaluation of different urban scenarios by Carlo et al. (2024) concluded that cars, boundary walls, and hedges along the pedestrian zones can reduce pollutant exposure by 15%, 23%, and 11%, respectively, while similarly located trees potentially increase exposure by 51% for dense and 17% for sparse tree arrangements.

To achieve more realistic results, some studies have examined either an idealized or an actual urban neighborhood. A study by Gromke and Blocken (2015a, 2015b) analyzed the impact of avenue trees in a simplified urban neighborhood comprising 7×7 building blocks through 3D steady Reynolds-averaged Navier-Stokes (RANS) simulations. It was concluded that a 1% increase in the vegetation coverage in the street canyons corresponded to about a 1% rise in neighborhood-average pollutant concentration, in the 4% to 14% coverage range.

Furthermore, air quality investigations were performed in real urban scenarios in Lisbon and Aveiro, Portugal (Amorim et al., 2013), as well as Pamplona, Spain (Santiago et al., 2017) through similar methods. Both studies revealed significant changes in the flow field due to the presence of trees,

with an average pollutant concentration increase from 7.2% up to 13.2% for perpendicular wind approach and 12% for oblique flows at pedestrian level.

Importantly, the majority of CFD-based research papers model the effects of vegetation via the solution of the Reynolds-averaged Navier-Stokes equation, a turbulence modelling approach frequently used in urban dispersion studies (Toparlar et al., 2017). The RANS approach has a few advantages compared to scale-resolving turbulence models, such as large eddy simulation (LES), namely that (1) its computational demand is significantly smaller than that of LES, and (2) there are numerous best practice guidelines (BPGs) available to support its use (Blocken and Gualtieri, 2012; Blocken, 2015). Therefore, it became common practice in both the industry and in research to employ the available computational power to simulate larger and more complex problems using RANS instead of switching to scale-resolving turbulence models (Blocken, 2018).

On the other hand, RANS results can often be inaccurate, both in urban dispersion studies (see, e.g., Gousseau et al., 2011; and Tominaga and Stathopoulos, 2013), and in other applications as well. It was noted by Kristóf et al. (2025) that in a quasi-stationary free shear flow, various well-known Reynolds-averaged turbulence models lead to qualitatively incorrect results: the velocity magnitude decreases over time, resulting in a decrease in the spatially averaged values of hydraulic power, production, and dissipation. However, when the driving force is maintained, the average value of turbulent kinetic energy remains close to the DNS results, indicating a realistic value. With nearly constant kinetic energy and decreasing dissipation, turbulent viscosity increases, which explains the reduction in velocity amplitude. Throughout this process, the turbulent length scale grows indefinitely. The incorrect asymptotic behavior of these models may also affect the accuracy of the engineering applications of CFD.

To address this issue, Kristóf et al. (2025) introduce a new eddy-viscosity formulation that depends on similar parameters to the k-ω SST model but includes an additional dependence on wall distance in the dissipative regime, proportional to the square root of the wall distance. This slight dependence on wall distance prevents the unlimited growth of the turbulent length scale, which is why we refer to the new formulation as the geometry-informed (GI) model. When incorporated into the standard k-ε model equations, the GI formulation yields a shear stress distribution in equilibrium channel flow that aligns well with known DNS results.

The resulting turbulence model (GI k-ε model) does not require wall function application (it is monotonically integrable from the wall) as long as the numerical grid is sufficiently refined near the solid wall ($y^+ \leq 4$).

The present paper aims to benchmark the new geometry-informed k-ε turbulence model in realistic urban applications, both in the presence of trees and in vegetation-free cases, by comparing the model results to data obtained using the industry standard RANS turbulence models and to the results of wind tunnel experiments.

2. METHODS

2.1. Geometry

A few geometries from the wind tunnel study by Carlo et al. (2024) were replicated using computational fluid dynamics (CFD) simulations. The investigated setup consisted of a regular array of $H = 0.1$ m tall, rectangular building blocks, forming numerous street canyons and intersections. The flow field is characterized by a Reynolds number of $Re = U_\infty H/\nu = 3 \times 10^7$. The street canyons parallel to the x axis (wind direction) have a height-to-width aspect ratio of $H/W = 1$, and the street canyons perpendicular to the wind direction have an aspect ratio of $H/W = 0.5$. Both types of street canyons are of $L/H = 5$ length. The modelled geometry is shown in Figure 1. The top boundary of the computational
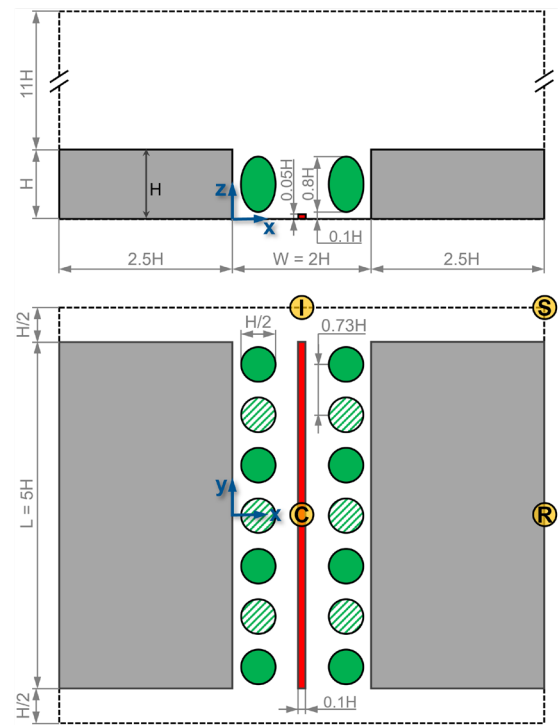

Figure 1. Layout and dimensions of the computational domain. The reference height is $H = 20$ m. In the *sparse trees* scenario (2×4 trees), the vegetation is only considered in the solid green zones, while in the *dense trees* setup (2×7 trees), vegetation is modelled in the zones denoted by both the solid and striped green areas. The yellow markers C (canyon), I (intersection), R (roof), and S (street) denote the location of the velocity profiles shown in Figure 3.

3

domain was placed $\delta = 11H$ distance above the rooftops, in which δ is the depth of the boundary layer forming above the building, as reported by Carlo et al. (2024) and Fellini et al. (2022).

Carlo et al. (2024) performed concentration measurements in one of the wider, $H/W = 0.5$ street canyons, located perpendicular to the wind direction, which is the critical orientation regarding air quality. In some cases, model trees were installed near the walkways on both sides. The *sparse trees* configuration consisted of four equidistantly placed trees on both sides of the canyon, while the *dense trees* setup had 2×7 trees installed (Figure 1). The wind tunnel experiments employed two parallel line sources in the middle of the canyon, which are modelled as a single combined emission zone in the present model, the length of which is equal to the length of the canyon ($L_s = L = 5H$).

2.2. Meshes and boundary conditions

The computational domain was discretized using polyhedral cells. The target cell size in the focus area, i.e., within the $H/W = 0.5$ canyon, was $H/\Delta x = 33$, with an additional mesh refinement to $H/\Delta x = 66$ near the source zone. The target mesh size was $H/16$ on every solid surface outside the target canyon. Inflation layers with a first layer height of $H/100$ were applied next to all solid boundaries. In the entire mesh, a linear growth rate of a maximum of 1.2 was allowed between adjacent cells, and the largest cells were $H/3$, near the top of the domain. The structure of the mesh is illustrated in Figure 2.

The above meshing parameters correspond to a medium mesh (hereinafter denoted by "M") of 2.04 million elements. Two further meshes were created using a linear refinement ratio, resulting in a coarser 1.01-million-cell and a more refined 5.33-million-
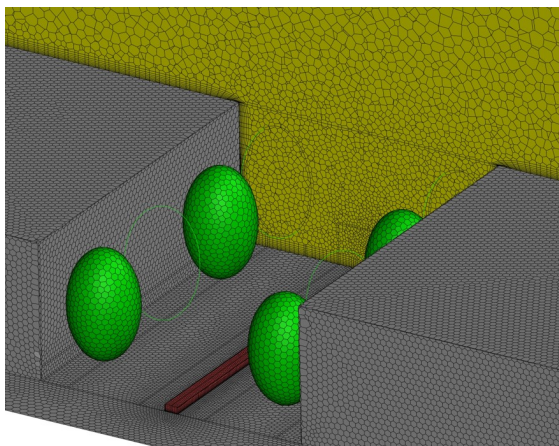

Figure 2. Spatial discretization of the computational domain near the buildings, for the coarsest mesh (S), with a spatial resolution of $H/\Delta x = 22$ within the canyon. The zones representing vegetation are denoted by green color. The pollutant source zone in the middle of the canyon is represented by red color. The yellow plane is an XZ cutplane located in the middle of the canyon ($y = 0$).

cell mesh, hereinafter denoted by "S" and "L", respectively. The orthogonal quality of the cells in each mesh was above 0.17, which is considered adequate.

To model the repetitive building pattern (see Fellini et al. (2022) and Carlo et al. (2024) for photos of the experimental setup), periodic boundary conditions were applied at the streamwise ends of the computational domain, and symmetry was assumed at the spanwise boundaries and at the top. At the solid boundaries, i.e., at the building walls, at its roof, and on the ground, rough no-slip walls were assumed, in combination with a near-wall treatment using the standard law of the wall. The equivalent sand-grain roughness (K_s) was set uniformly for all walls in each simulation to have a good match with the TKE profile obtained above the buildings in the wind tunnel.

The periodic model was driven by a pressure gradient in the x direction, controlled around the value of –0.08 Pa/m with a prescribed target mass flow rate of air in the x direction of 3.9 kg/s. The mass flow rate was prescribed in order to result in a free-stream velocity of $U_\infty = u(\delta) \approx 5.5$ m/s, in line with the measurements of Carlo et al. (2024).

Importantly, while the flow field is periodic, the concentration field is not: we only want to model the pollutants emitted in the investigated canyon, and no upstream sources are taken into account – similarly to the wind tunnel experiments. Consequently, the flow and concentration fields must be computed separately. After reaching sufficient convergence for the former, the periodic boundaries were decoupled, and the flow field was "frozen", i.e., only the diffusion equation was solved, taking the flow field as an input. For this, a pressure outlet boundary condition is assumed at the downstream boundary (with 0 Pa gauge pressure), allowing the pollutants to leave the simulation domain freely.

2.3. Solver setup

In the majority of the cases presented in this paper, the geometry-informed k-ε model developed by Kristóf et al. (2025) was applied. For comparison, turbulence was also modelled using the realizable k-ε model, which is considered the industry standard approach for steady-state RANS calculations in the field of urban dispersion. Furthermore, the k-ω SST model, widely used in several engineering applications, was also utilized in one simulation.

The dispersion of traffic-related air pollutants was modelled using a passive scalar. The pollutant source was represented by a volume source term, S_V, added to the scalar transport equations. The pollutant emission rate, therefore, can be calculated as $Q = S_V/(\rho V_s)$, in which ρ is the density of air, and V_s is the total volume of the source zones.

Setting an appropriate value for the turbulent Schmidt number, i.e., the ratio of the turbulent viscosity to the turbulent mass diffusivity

4

($Sc_t = \nu_t/D_t$), can strongly influence the quality of the concentration results calculated based on steady-state RANS models (Gousseau et al., 2011). In the present study, $Sc_t = 0.2$ was chosen for all cases, via optimization over the $Sc_t = 0.04…1.3$ range. According to Tominaga and Stathopoulos (2007), the found optimum value is lower than usually applied in near-field dispersion, but not unprecedented, see e.g., He et al. (1999).

The transport equations were solved using the Coupled solver and second order flux schemes for the spatial discretization of all variables in Ansys Fluent 2023R1. Due to the high characteristic Reynolds number, the limit for the turbulent viscosity ratio was increased to 10^{20}, which is a common practice in building-scale RANS calculations.

2.4. Modelling the effects of vegetation

The effect of vegetation was modelled using the following source terms in the vegetation zones (see Figure 1 and Figure 2) for the flow and turbulence equations, following the model derived by Sanz (2003).

$$S_{u,i} = -\rho c_d u_i |\mathbf{v}| \tag{1}$$

$$S_k = \rho c_d \left(\beta_p |\mathbf{v}|^3 - \beta_d |\mathbf{v}| k \right) \tag{2}$$

$$S_\varepsilon = \rho c_d \frac{\varepsilon}{k} \left(C_{\varepsilon 4} \beta_p |\mathbf{v}|^3 - C_{\varepsilon 5} \beta_d |\mathbf{v}| k \right) \tag{3}$$

In the above equations, $S_{u,i}$, S_k, and S_ε are the source terms appearing in the transport equations for the three velocity components ($u_i = u, v, w$) as well as for the turbulent kinetic energy (k) and its dissipation rate (ε). Furthermore, ρ is the density of air, $c_d = 0.65$ is the drag coefficient of a single tree (Carlo et al., 2024), and $|\mathbf{v}|$ denotes the magnitude of the velocity vector. Finally, $\beta_p = 1$, $\beta_d = 5.1$, $C_{\varepsilon 4} = 0.9$, and $C_{\varepsilon 5} = 0.9$ are model constants.

The source terms in the momentum equation account for the pressure loss caused by the viscous resistance of the tree branches and the leaves. Moreover, the source term in the transport equation of k models the conversion of large-scale TKE into small-scale TKE, as the porous canopy converts the energy of the flow into wake turbulence. Finally, source term for the turbulent dissipation is based on Kolmogorov's relation (Balogh and Kristóf, 2009).

The above formulation is widely used in the literature, such as by Balogh and Kristóf (2009), Balczó et al., (2009), Kenjeres and Ter Kuile (2013), Gromke and Blocken (2015a, 2015b), and Santiago et al. (2019). It is important to note that the values of the parameters (β_p, β_d, $C_{\varepsilon 4}$, and $C_{\varepsilon 5}$) can vary between different studies, and the values used in the present model are taken from Gromke et al. (2015a).

For fellow CFD modelers, we have two practical remarks. Firstly, if the geometry is created in model scale, the full-scale drag coefficient of a single tree must be multiplied by the model scale to yield the same pressure loss – see Balczó et al. (2009) and Gromke (2011). Secondly, for sufficient convergence, the use of an implicit solver is required. Therefore, the derivatives of the above source terms with respect to u_i, k, and ε must be provided – see, e.g., Balczó et al. (2009).

2.5. Performance metrics

To assess the accuracy of the models, the performance metrics proposed by Chang and Hanna (2004) were applied to the concentration results. The full names of the metrics are given in Table 1 later.

$$R = \frac{\overline{\left(O - \overline{O} \right) \left(P - \overline{P} \right)}}{\sigma_O \, \sigma_P} \tag{4}$$

$$FAC2 = \frac{1}{N} \sum_{i=1}^{N} f_i, \quad with$$

$$f_i = \begin{cases} 1 & if \quad 0.5 \le \dfrac{P_i}{O_i} \le 2 \\ 0 & otherwise \end{cases} \tag{5}$$

$$FB = \frac{\overline{O} - \overline{P}}{0.5 \left(\overline{O} + \overline{P} \right)} \tag{6}$$

$$NMSE = \frac{\overline{(O - P)^2}}{\overline{O} \, \overline{P}} \tag{7}$$

$$MG = \exp\left(\overline{\ln O} - \overline{\ln P} \right) \tag{8}$$

$$VG = \exp\left(\overline{(\ln O - \ln P)^2} \right) \tag{9}$$

In addition to the above performance metrics, the average absolute deviation, as defined by Montazeri and Blocken (2013), can be computed as

$$AAD = \overline{|O - P|}. \tag{10}$$

In the above formulas, P denotes the model predictions (CFD simulation results), and O denotes the reference data observed in the experiments. Moreover, $\overline{O}$ and $\overline{P}$ stand for the averages over these data sets, σ_O and σ_P represent their standard deviations, and N denotes the number of elements of the data sets. Note that as the absolute measurement uncertainty is unknown, small data are not omitted based on this criterion; hence, the formulas presented in this paper are mathematically simpler than the original ones.

3. RESULTS AND DISCUSSION

This section presents the comparison of the velocity, turbulence, and concentration results obtained throughout seven simulation cases, with combinations of (1) three meshes of different spatial

resolution, (2) three turbulence models and two different wall roughnesses, and (3) three different tree configurations, including the tree-free canyon.

3.1. The impact of the applied turbulence model on the flow and concentration field

Firstly, let us compare the flow fields obtained using different turbulence models. As discussed above, the wall roughness was tuned to achieve a good agreement between the numerical and experimental TKE profiles. As shown in Figure 3, the geometry-informed k-ε model requires around two times higher sand-grain roughness ($K_s/H = 0.15$) to achieve the same turbulence levels compared to the realizable k-ε and the k-ω SST models ($K_s/H = 0.07$). It is also worth noting that the GI k-ε model reproduces the shape of the TKE profile most accurately, especially just above roof height. The agreement of the GI k-ε model results and the experimental data is characterized by NMSE = 6.7×10^{-3} in contrast to 1.1×10^{-2} (realizable k-ε) and 1.8×10^{-2} (k-ω SST). Moreover, despite the fact that the TKE in the bulk flow is set to be similar for all turbulence models, the GI k-ε model yields substantially more turbulence below roof height, which is also visible in Figure 5.

Furthermore, let us assess the shape of the velocity profiles. It can be clearly seen that the GI k-

ε model (with $K_s/H = 0.15$) yields the closest match with the experimental results, characterized by NMSE = 5.9×10^{-3} (averaged over the four velocity profiles shown in Figure 3), while the realizable k-ε and the k-ω SST models yield somewhat more modest values (8.3×10^{-3} and 1.7×10^{-2}, respectively). The agreement of the profiles produced by the GI k-ε model is remarkable in the lower part of the "intersection" location, but the three other velocity profiles show similar levels of correspondence, too. Note that all CFD profiles show excellent correlation with the experimental data: the correlation coefficients are over R = 0.98 for each profile.

Secondly, the concentration results presented in Figure 4, obtained using $Sc_t = 0.2$, show a good agreement between the experimental observations and the model predictions in 116 gauging points located within the canyon. It was observed that for higher Sc_t values, the model overpredicts the concentrations for all investigated turbulence models. This draws attention to the fact that the applied periodic modelling approach combined with RANS turbulence models requires setting a lower Sc_t value than usually applied in near-field dispersion studies.

The performance metrics of the concentration results, compiled in Table 1, highlight that although all three models show only acceptable correlation with the experimental data (R = 0.517…0.543), the
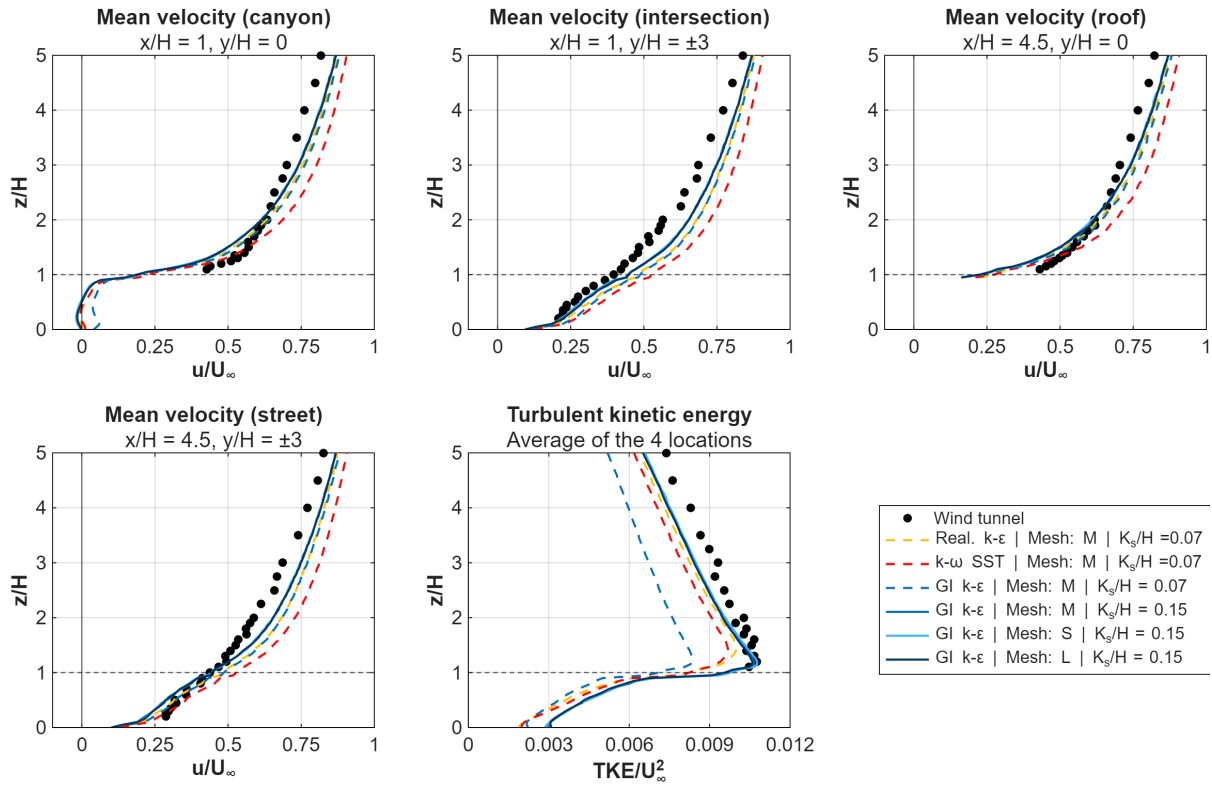

Figure 3. Comparison of the velocity and turbulence profiles obtained in the numerical simulations using turbulence models and meshes and in the wind tunnel experiments by Fellini et al. (2022) and Carlo et al. (2024). The locations of the four vertical profiles are shown in Figure 1. (In this figure, the profiles are only shown up to z/H = 5, but they were modelled up to z/H = 12.)
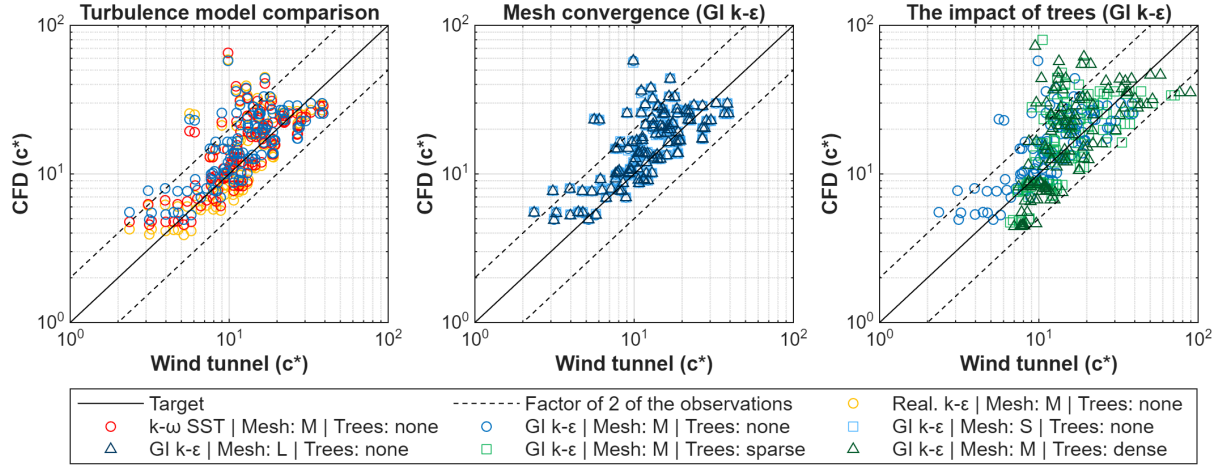
Figure 4. Comparison of the mean normalized concentration ($c^* = cU_\infty L_s H / Q$) obtained in the 116 gauging points of the wind tunnel experiments by Carlo et al. (2024) and the corresponding locations in the CFD simulations of the present study.

systematic error is minor, (FB = 0.171…0.240, MG = 1.137…1.281) and the scatter of the data is also moderate (NMSE = 0.339…0.351, VG = 1.219…1.263). The average absolute deviation of the predicted concentrations from the measured ones is AAD = 5.3…5.9 for the three different turbulence models, which can be considered acceptable, as the range of the experimentally observed concentrations for the empty street canyon was $c^* = 2.4…39.0$.

In conclusion, it can be stated that the geometry-informed k-ε turbulence model is capable of reproducing the flow and concentration field in urban street canyons with similar accuracy as the industry standard realizable k-ε and k-ω SST models.

3.2. Mesh convergence analysis

It can be observed in Figure 3 that the velocity and TKE profiles obtained using different spatial resolutions (within the canyon: $H/22$, $H/33$, $H/50$), shown by the three continuous blue curves, collapse onto one another within a line width. Furthermore,

the dispersion results shown in the middle panel of Figure 4 reveal that the concentrations obtained at each gauging point on the different meshes are very close to one another, i.e., the resulting scatter plots show a very good overlap.

The above findings are also reinforced by the performance metrics presented in Table 1: the values of the metrics do not significantly change with the mesh refinement, supporting the conclusion that even a $H/22$ spatial resolution within the canyon is sufficient for steady-state RANS simulations of urban dispersion using the geometry-informed k-ε model.

3.3. The impact of trees on urban air quality

The scatter plots presented in the right-hand panel of Figure 4 reveal that qualitatively, the agreement with the measurement data is similar to that of the treeless case. Moreover, the performance metrics presented in Table 1 show minor improvements in terms of the systematic error (see FB and MG), but the noticeable

Table 1. Performance metrics characterizing the performance of the dispersion model in combination with different meshes, turbulence models and tree configurations. (The formulas for the metrics are given in Eqs. 4-10.)

Tree configuration ▶	none					sparse	dense	Target
Turbulence model ▶	real. k-ε	k-ω SST	geometry-informed k-ε					
Metric ▼ Mesh ▶	M			S	L	M		
Correlation coefficient (R)	0.543	0.522	0.517	0.523	0.516	0.422	0.456	1
Factor of two of observations (FAC2)	0.914	0.888	0.862	0.862	0.862	0.836	0.828	1
Fractional bias (FB)	0.171	0.181	0.240	0.235	0.240	0.136	0.163	0
Geometric mean bias (MG)	1.137	1.181	1.281	1.277	1.281	1.083	1.093	1
Normalized mean square error (NMSE)	0.351	0.345	0.339	0.331	0.341	0.488	0.583	0
Geometric variance (VG)	1.237	1.219	1.263	1.259	1.263	1.304	1.391	1
Average absolute deviation (AAD)	5.521	5.319	5.941	5.867	5.955	8.286	9.635	0

increase of the NMSE, VG, and AAD values suggests that the model predictions of pointwise concentration values are more intensely affected by the random error when vegetation is present. Nevertheless, all metrics can be considered moderate; therefore, the geometry-informed k-ε turbulence model can be viewed as a reasonable alternative for predicting the concentration field in the presence of trees as well.
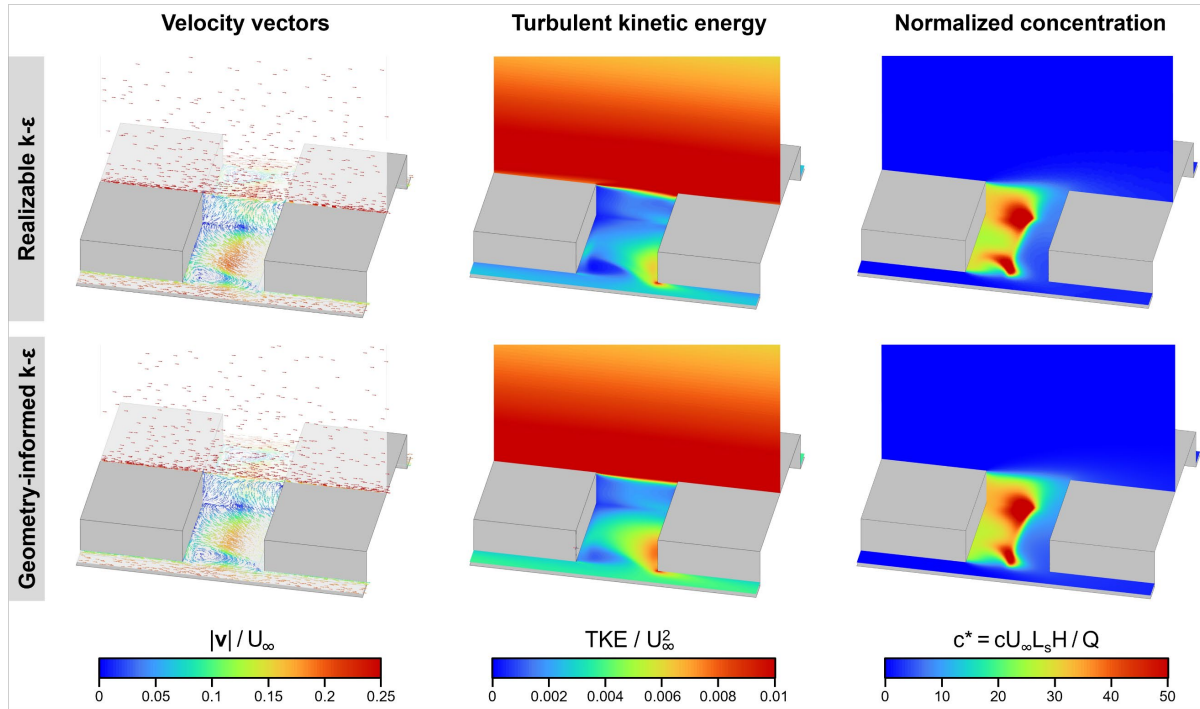

Figure 5. Comparison of the flow and concentration fields obtained using the realizable k-ε model and the geometry-informed k-ε model on the medium-resolution mesh (M). The vertical cut-plane is located at the symmetry plane ($y = 0$), and the horizontal cutplane is located at $z/H = 0.1$.
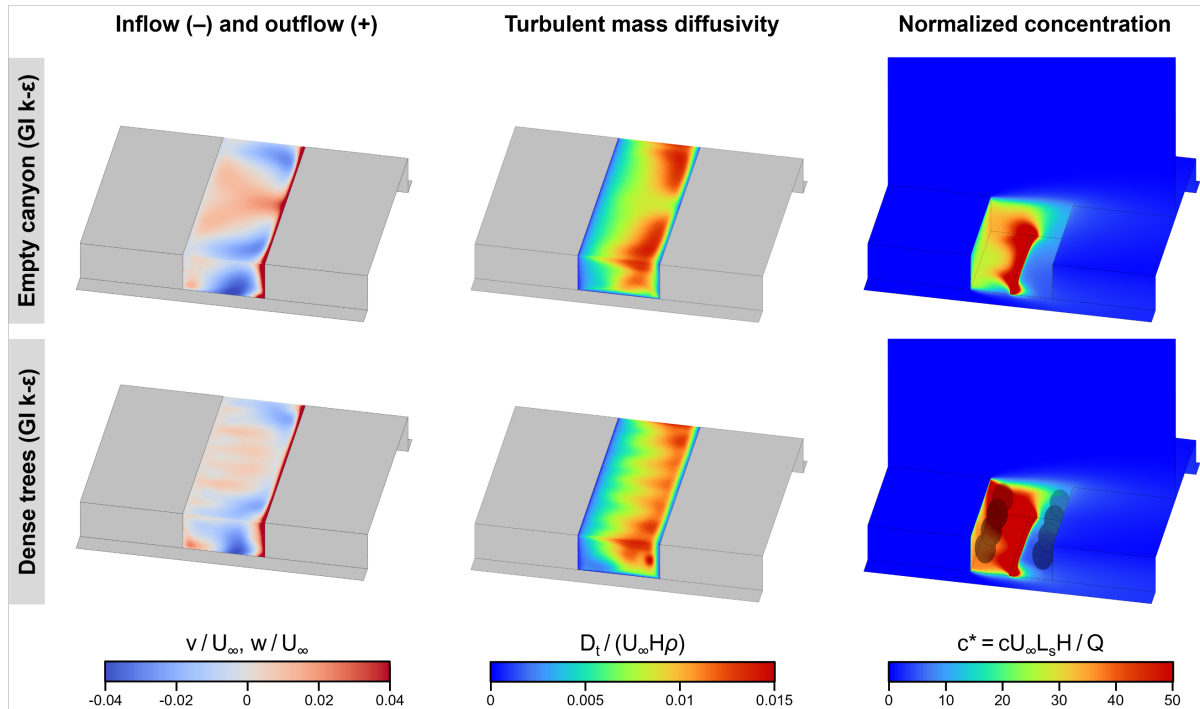
Figure 6. Comparison of the quantities characterizing the transport processes, both for an empty street canyon and one with densely installed trees. The concentration is plotted on the walls and a vertical cut-plane located at the symmetry plane ($y = 0$). All results in this figure were obtained using the geometry-informed k-ε model.

8

To the best of the Authors' knowledge, no CFD results were previously published for the currently investigated geometry; therefore, a handful of simulation results are hereby presented in order to provide aid in understanding the flow and dispersion processes governing the mass transfer of medium-length street canyons.

The left-hand-side panels of Figure 6 show that the presence of trees substantially decreases the magnitude of the inflow and outflow velocities at the lateral sides of the canyon, and especially at roof level, above both the leeward and the windward walkways. Similarly, the turbulent mass diffusivity at the lateral and vertical boundaries of the canyon, becomes noticeably lower when 2×7 trees are present (i.e., for the dense tree arrangement), resulting in an increase in pedestrian exposure by 31.6% over the leeward (upwind) walkway and a decrease of 9.4%, over the windward (downwind) walkway. Remark: the spatial averages were obtained in $0.1H$ tall and $0.2H$ wide boxes at the feet of the buildings. Although the concentration decrease at the windward pedestrian zone of the vegetated street canyon may sound counterintuitive, Carlo et al. (2024) reported similar findings in the experiments.

The predicted concentration changes in the pedestrian zones and in the entire canyon relative to the tree-free canyon are listed in Table 2 for both tree configurations. The currently presented model results somewhat underestimate the observations of Carlo et al. (2024), who found the canyon-average concentration to increase by 22.3% and 70.5% as the consequence of planting the trees in the sparse and dense configurations, respectively, based on the average of the pointwise measurements.

4. CONCLUSIONS AND OUTLOOK

In this paper, a novel RANS turbulence model, the geometry-informed k-ε (GI k-ε) model developed by Kristóf et al. (2025), was applied to simulate the time-averaged flow and concentration field in a periodic building configuration. The investigated geometry consisted of street canyons of $H/W = 0.5$ and $L/H = 5$, in which the effects of 2×4 and 2×7 trees, installed over the walkways, on urban air quality and pedestrian exposure were also analyzed.

The results underline that the new geometry-informed k-ε turbulence model is a suitable alternative for computing the flow and dispersion field to the industry standard realizable k-ε and k-ω SST turbulence models based on several performance metrics. It was also shown that the GI k-ε model results are of similar accuracy for the two tree arrangements of different density as for an empty street canyon, with the relative concentration increases due to the presence of vegetation also being generally in line with the experimental observations of Carlo et al. (2024) about the same setup.

In its current form, the GI k-ε model differs from the standard k-ε model primarily in the formulation of the eddy viscosity. The optimization of the source terms in the turbulent dissipation (ε) transport equation is the subject of ongoing research. However, even in its present state, the model represents a reasonable alternative approach for simulating urban air pollutant dispersion, and its further development is worth paying attention to.

REFERENCES

Amorim, J. H., Rodrigues, V., Tavares, R., Valente, J., & Borrego, C. (2013). CFD modelling of the aerodynamic effect of trees on urban air pollution dispersion. Science of the Total Environment, 461, 541-551. CFD modelling of the aerodynamic effect of trees on urban air pollution dispersion (2013). Sci. Total Environ. 461–462, 541–551. https://doi.org/10.1016/j.scitotenv.2013.05.031

Table 2. The impact of trees on urban air quality: changes in the volume-averaged normalized concentration ($c^* = cU_\infty L_s H / Q$) in both pedestrian zones and in the entire canyon.

	Leeward pedestrian zone		Windward pedestrian zone		Canyon average	
	c^* (–)	Δc^* (%)	c^* (–)	Δc^* (%)	c^* (–)	Δc^* (%)
Empty canyon	28.0	N/A	6.9	N/A	16.9	N/A
Sparse trees	34.9	19.9%	6.5	-6.5%	19.6	14.1%
Dense trees	40.9	31.6%	6.3	-9.4%	21.3	21.0%

Ansys, Inc. (2023). Ansys Fluent User's Guide, release 2023R1. Ansys, Inc., Canonsburg, PA.

Balczó, M., Gromke, C., & Ruck, B. (2009). Numerical modelling of flow and pollutant dispersion in street canyons with tree planting. Meteorologische Zeitschrift, 197–206. https://doi.org/10.1127/0941-2948/2009/0361

Balogh, M., & Kristóf, G. (2009). Fine scale simulation of turbulent flows in urban canopy layers. Időjárás – Quarterly Journal of the Hungarian Meteorological Service. Vol. 114, No. 1–2, pp. 135–148.

Blocken, B. (2015). Computational Fluid Dynamics for urban physics: Importance, scales, possibilities, limitations and ten tips and tricks towards accurate and reliable simulations. Building and Environment, 91, 219–245. https://doi.org/10.1016/j.buildenv.2015.02.015

Blocken, B. (2018). LES over RANS in building simulation for outdoor and indoor applications: A foregone conclusion? Building Simulation, 11(5), 821–870. https://doi.org/10.1007/s12273-018-0459-3

Blocken, B., & Gualtieri, C. (2012). Ten iterative steps for model development and evaluation applied to Computational Fluid Dynamics for Environmental Fluid Mechanics. Environmental Modelling & Software, 33, 1–22. https://doi.org/10.1016/j.envsoft.2012.02.001

Buccolieri, R., Gromke, C., Di Sabatino, S., Ruck, B. (2009). Aerodynamic effects of trees on pollutant concentration in street canyons. Sci. Total Environ. 407(19), 5247–5256. https://doi.org/10.1016/j.scitotenv.2009.06.016

Buccolieri, R., Santiago, J.-L., Rivas, E., Sanchez, B. (2018). Review on urban tree modelling in CFD simulations: Aerodynamic, deposition and thermal effects. Urban For. Urban Green. 31, 212–220. https://doi.org/10.1016/j.ufug.2018.03.003

Carlo, O. S., Fellini, S., Palusci, O., Marro, M., Salizzoni, P., Buccolieri, R. (2024). Influence of obstacles on urban canyon ventilation and air pollutant concentration: An experimental assessment. Build. Environ. 250, 111143. https://doi.org/10.1016/j.buildenv.2023.111143

Chang, J. C., & Hanna, S. R. (2004). Air quality model performance evaluation. Meteorology and Atmospheric Physics, 87(1–3). https://doi.org/10.1007/s00703-003-0070-7

Fellini, S., Marro, M., Del Ponte, A. V., Barulli, M., Soulhac, L., Ridolfi, L., Salizzoni, P. (2022). High resolution wind-tunnel investigation about the effect of street trees on pollutant concentration and street canyon ventilation. Build. Environ. 226, 109763. https://doi.org/10.1016/j.buildenv.2022.109763

Gallagher, J., Baldauf, R., Fuller, C. H., Kumar, P., Gill, L. W., & McNabola, A. (2015). Passive methods for improving air quality in the built environment: A review of porous and solid barriers. Atmospheric environment, 120, 61-70. Passive methods for improving air quality in the built environment: A review of porous and solid barriers (2015). . Atmos. Environ. 120, 61–70. https://doi.org/10.1016/j.atmosenv.2015.08.075

Gill, S. E., Handley, J. F., Ennos, A. R., Pauleit, S., Theuray, N., & Lindley, S. J. (2008). Characterising the urban environment of UK cities and towns: A template for landscape planning. Landscape and urban planning, 87(3), 210-222. Characterising the urban environment of UK cities and towns: A template for landscape planning (2008). Landsc. Urban Plan. 87(3), 210–222. https://doi.org/10.1016/j.landurbplan.2008.06.008

Gómez-Baggethun, E., Gren, Å., Barton, D. N., Langemeyer, J., McPhearson, T., O'Farrell, P., Andersson, E., Hamstead, Z., Kremer, P. (2013). Urban Ecosystem Services, in: Elmqvist, T., Fragkias, M., Goodness, J., Güneralp, B., Marcotullio, P. J., McDonald, R. I., Parnell, S., Schewenius, M., Sendstad, M., Seto, K. C., Wilkinson, C. (Eds.), Urbanization, Biodiversity and Ecosystem Services: Challenges and Opportunities. Springer Netherlands, Dordrecht, 175–251. https://doi.org/10.1007/978-94-007-7088-1_11

Gousseau, P., Blocken, B., Stathopoulos, T., & van Heijst, G. J. F. (2011). CFD simulation of near-field pollutant dispersion on a high-resolution grid: A case study by LES and RANS for a building group in downtown Montreal. Atmospheric Environment, 45(2), 428–438. https://doi.org/10.1016/j.atmosenv.2010.09.065

Gromke, C. (2011). A vegetation modelling concept for Building and Environmental Aerodynamics wind tunnel tests and its application in pollutant dispersion studies. Environmental Pollution, 159(8–9), 2094–2099. https://doi.org/10.1016/j.envpol.2010.11.012

Gromke, C., Blocken, B. (2015a). Influence of avenue-trees on air quality at the urban neighborhood scale. Part I: Quality assurance studies and turbulent Schmidt number analysis

for RANS CFD simulations. Environ. Pollut. 196, 214–223. https://doi.org/10.1016/j.envpol.2014.10.016

Gromke, C., Blocken, B. (2015b). Influence of avenue-trees on air quality at the urban neighborhood scale. Part II: Traffic pollutant concentrations at pedestrian level. Environ. Pollut. 196, 176–184. https://doi.org/10.1016/j.envpol.2014.10.015

He, G., Guo, Y., & Hsu, A. T. (1999). The effect of Schmidt number on turbulent scalar mixing in a jet-in-crossflow. International Journal of Heat and Mass Transfer, 42(20), 3727–3738. https://doi.org/10.1016/S0017-9310(99)00050-2

Janhäll, S. (2015). Review on urban vegetation and particle air pollution – Deposition and dispersion. Atmos. Environ. 105, 130–137. https://doi.org/10.1016/j.atmosenv.2015.01.052

Kenjereš, S., & Ter Kuile, B. (2013). Modelling and simulations of turbulent flows in urban areas with vegetation. Journal of Wind Engineering and Industrial Aerodynamics, 123, 43–55. https://doi.org/10.1016/j.jweia.2013.09.007

Kristóf, G., Kovács, K. A., Kalmár-Nagy, T., and Balogh, M. (2025). A New Viscosity Formulation for Improved Turbulence Modelling in Kolmogorov Flow. Conference on Modelling Fluid Flow (CMFF'25), Budapest, Hungary.

Montazeri, H., & Blocken, B. (2013). CFD simulation of wind-induced pressure coefficients on buildings with and without balconies: Validation and sensitivity analysis. Building and Environment, 60, 137–149. https://doi.org/10.1016/j.buildenv.2012.11.012

Papp, B., Kristóf, G., Istók, B., Koren, M., Balczó, M., & Balogh, M. (2021). Measurement-driven Large Eddy Simulation of dispersion in street canyons of variable building height. Journal of Wind Engineering and Industrial Aerodynamics, 211, 104495. https://doi.org/10.1016/j.jweia.2020.104495

Salmond, J. A., Tadaki, M., Vardoulakis, S., Arbuthnott, K., Coutts, A., Demuzere, M., Dirks, K. N., Heaviside, C., Lim, S., Macintyre, H., McInnes, R. N., Wheeler, B. W. (2016). Health and climate related ecosystem services provided by street trees in the urban environment. Environ. Health 15(1), 95–111. https://doi.org/10.1186/s12940-016-0103-6

Santiago, J.-L., Buccolieri, R., Rivas, E., Calvete-Sogo, H., Sanchez, B., Martilli, A., Alonso, R., Elustondo, D., Santamaría, J. M., & Martin, F. (2019). CFD modelling of vegetation barrier effects on the reduction of traffic-related pollutant concentration in an avenue of Pamplona, Spain. Sustainable Cities and Society, 48, 101559. https://doi.org/10.1016/j.scs.2019.101559

Santiago, J.-L., Rivas, E., Sanchez, B., Buccolieri, R., Martin, F. (2017). The Impact of Planting Trees on NOx Concentrations: The Case of the Plaza de la Cruz Neighborhood in Pamplona (Spain). Atmosphere 8(7), 131. https://doi.org/10.3390/atmos8070131

Sanz, C. (2003). A Note on k—ε Modelling of Vegetation Canopy Air-Flows. Boundary-Layer Meteorology, 108(1), 191–197. https://doi.org/10.1023/A:1023066012766

Tominaga, Y., & Stathopoulos, T. (2007). Turbulent Schmidt numbers for CFD analysis with various types of flowfield. Atmospheric Environment, 41(37), 8091–8099. https://doi.org/10.1016/j.atmosenv.2007.06.054

Tominaga, Y., & Stathopoulos, T. (2013). CFD simulation of near-field pollutant dispersion in the urban environment: A review of current modelling techniques. Atmospheric Environment, 79, 716–730. https://doi.org/10.1016/j.atmosenv.2013.07.028

Toparlar, Y., Blocken, B., Maiheu, B., & van Heijst, G. J. F. (2017). A review on the CFD analysis of urban microclimate. Renewable and Sustainable Energy Reviews, 80, 1613–1640. https://doi.org/10.1016/j.rser.2017.05.248